INL/JOU-23-74264-Revision-0

Stochastic Optimization and Uncertainty Quantification of Natrium-based Nuclear-Renewable Energy Systems for Flexible Power Applications in Deregulated Markets

Manjur Basnet, Jacob Bryan, Seth Dana, Aiden Meek, Hailei Wang, Paul W Talbot

Changing the World's Energy Future

Idaho National Laboratory

INL is a U.S. Department of Energy National Laboratory operated by Battelle Energy Alliance, LLC

INL/JOU-23-74264-Revision-0

Stochastic Optimization and Uncertainty Quantification of Natrium-based Nuclear-Renewable Energy Systems for Flexible Power Applications in Deregulated Markets

Manjur Basnet, Jacob Bryan, Seth Dana, Aiden Meek, Hailei Wang, Paul W Talbot

December 2024

Idaho National Laboratory
Idaho Falls, Idaho 83415

http://www.inl.gov

Prepared for the
U.S. Department of Energy
Under DOE Idaho Operations Office
Contract DE-AC07-05ID14517

Received: Added at production | Revised: Added at production | Accepted: Added at production

DOI: xxx/xxxx

RESEARCH ARTICLE

Sensitivity Analysis of a Nuclear Hybrid Energy System with Thermal Energy Storage in Deregulated Electricity Markets Considering Time Series Uncertainty in Electricity Price

Jacob A. Bryan[1] | **Hailei Wang**[1] | **Paul W. Talbot**[2]

[1]Department of Mechanical and Aerospace Engineering, Utah State University, Utah, USA

[2]Idaho National Laboratory, Idaho, USA

Correspondence
Corresponding author: Jacob A. Bryan
Email: jacob.bryan@usu.edu

Funding Information
This research was supported by the U.S. Department of Energy Nuclear Energy University Program, Award Number: DE-NE0009159.

Abstract

Adding thermal energy storage to nuclear power plants has been proposed as a way to allow nuclear plants to operate more flexibly and potentially be more competitive in deregulated electricity markets. The economics of these systems in deregulated markets are subject to uncertainties in capital costs, operating costs, and revenue. This study quantifies the uncertainty in the net present value of a nuclear power plant with integrated thermal energy storage in three U.S. deregulated electricity markets considering these sources of uncertainty and quantifies, for the first time, the relative contributions each source makes to the overall uncertainty. To accomplish this, a computationally efficient block bootstrap method is introduced to quantify uncertainty contributions from the stochastic time series of electricity prices, achieving a two order of magnitude decrease computational time compared to the model-based methods used in previous works while also relaxing several strict assumptions made by the model-based approach. Up to 18.5% of the overall variance in net present value is attributable to variance in the electricity price stochastic process, with this sensitivity varying significantly across markets.

KEYWORDS
Integrated energy system, Hybrid energy system, Sensitivity analysis, Uncertainty quantification, Advanced nuclear, Thermal energy storage, Deregulated electricity markets

1 | INTRODUCTION

The United States has set the goals of achieving a 100% clean electricity grid by 2035 and economy-wide net-zero greenhouse gas emissions by 2050 [1]. Generator-side pathways to achieving this 2035 goal rely on a broad mix of electricity generation resources, including wind, solar, nuclear, energy storage, carbon capture and other net-zero energy sources [2]. Wind and solar power are essential components of a net-zero electricity system, but they are intermittent resources that are not economical or feasible for every region. Furthermore, greater penetration of these renewable energy resources in some regions has resulted in increased volatility in net electricity demand and decreased the minimum baseload generation required to meet this demand [3].

Nuclear power plants (NPPs) have historically operated as baseload electricity providers, given their ability to provide firm, consistent power output regardless of weather or time of day. Many of these plants have responded to this increased volatility in their respective electricity markets by operating more flexibly, reducing power output during low-demand periods, though this type of load-following operation is not currently allowed by regulating bodies in all regions [4]. However, reducing power output at a nuclear power plant does not reduce the plant's operating

costs; the only economic benefit to reducing power output lies in avoiding the sale of generated electricity at negative prices [5]. Integrated energy systems (IES) seek to add flexibility to nuclear plants by providing other avenues for using the heat and electricity generated by the plants, such as storing energy in coupled thermal energy storage systems, providing heat for industrial processes, or producing other commodities like hydrogen [6, 7, 8]. Enabling the energy system to quickly follow electricity demand and price to optimally allocate its resources may lead to increased profitability of these systems compared to reference plants with less flexibility.

Nuclear power plants with integrated thermal energy storage (TES) are a current subject of industrial interest, as shown by the Natrium plant designed by TerraPower and GE Hitachi Nuclear Energy [9]. Natrium is a 345-MW_e nuclear power plant with gigawatt-scale molten salt thermal energy storage, allowing the system output to produce up to 500 MW_e for 5.5 hours without changing the thermal output of the reactor. Deregulated electricity markets, which serve electricity demand in their respective regions through competitive markets into which generators bid their capacity [10], are of particular interest for this type of flexible nuclear power plant because nuclear power plants have become decreasingly cost-competitive with coal and natural gas as electricity sources in these markets [11].

Due to stochastic variation in electricity demand, variable renewable energy generation, and other sources of supply-side or demand-side uncertainties in the market, the hourly day-ahead price of electricity paid to generators in deregulated electricity markets exhibits significant variability, with daily, weekly, and seasonal periodicities and large but infrequent spikes in price. This stochasticity in the electricity price causes uncertainty in the expected revenue for generators participating in these markets. Previous studies of the economics of advanced nuclear reactors tend to focus on the costs of the plants, such as capital expenses (CAPEX) and operating expenses (OPEX), but do not contextualize these costs with expected revenue [12, 13]. Other studies, such as those in Refs. [14, 15], consider the contributions of electricity price uncertainty to NPV for their respective IES designs but fail to include CAPEX and OPEX uncertainties when quantifying that uncertainty in NPV. Hill et al. [16] quantify the uncertainty in levelized cost of electricity (LCOE) of a nuclear power plant with thermal energy storage due to uncertainties in system component CAPEX and OPEX and variability in electricity demand, wind power, and solar power over a 6-month period in the California market (CAISO). However, their study does not quantify the relative contribution of these uncertainties to overall uncertainty in LCOE, and the uncertainties in revenue which would be present for an energy system operating in CAISO, a deregulated electricity market, are not considered.

The present study extends the work of Ref. [15] to include uncertainty in nuclear power plant CAPEX and OPEX and thermal energy storage CAPEX. This study also builds upon Ref. [16] by expanding the analysis to 3-5 years of historical data from the California, Texas, and Midcontinent U.S. electricity markets (CAISO, ERCOT, and MISO, respectively). The expansion to multiple years and regions has two-fold motivation. First, the large but infrequent spikes in electricity price are a significant statistical feature of the price time series. Expanding to multiple years of data allows for better quantification of the effects of these price spikes on the NPV of the IES of interest. Second, the statistical behavior of the electricity price is not uniform across regions; each market is unique, and so the market-related uncertainties in each region will be different. Considering multiple markets demonstrates this non-uniformity in uncertainty.

Finally, the previous studies of Refs. [14, 15, 16] and others all use a Monte Carlo uncertainty quantification approach which uses ARMA-based time series models for quantifying uncertainty from time series sources. However, the repeated sampling and optimization process required by this method is needlessly computationally demanding for many analyses. This study introduces a bootstrap-based approach which reduces the computation time for this task by two orders of magnitude while relaxing assumptions of the electricity price distribution and autocorrelation function made by the ARMA-based approaches and achieving better estimation of revenue uncertainty.

The remainder of this study is presented as follows. Section 2 exhibits the time series data collected from the CAISO, ERCOT, and MISO markets considered in this study. Three to five years of historical electricity price data is collected from each region, depending on data availability. Section 3 reviews cost estimates of the capital costs and operating costs for advanced nuclear power plants and two-tank molten salt thermal energy storage systems. In Section 4, a numerical model for a nuclear power plant with thermal energy storage is devised. The specifications of the modeled system are inspired by the Natrium design. The ARMA-based and bootstrap-based time series uncertainty quantification approaches are described in Section 5. A semi-analytical method for calculating Sobol sensitivity indices for uncertain cash flows is also presented in Section 5. The results of the sensitivity analysis are

presented in Section 6, where the Sobol indices for each market and the distributions of increase in revenue are presented. The main findings of the study are summarized in Section 7.

2 | HISTORICAL DATA FROM US ISOS

There are seven deregulated electricity markets in the United States: New York (NYISO), New England (ISO-NE), Pennsylvania-Jersey-Maryland (PJM), Midcontinent (MISO), the Southwest Power Pool (SPP), Texas (ERCOT), and California (CAISO). Of these markets, three have been selected as markets of interest due to their varying levels of renewable energy capacity. ERCOT is the nation's leader in wind energy, having produced 107 TWh of electricity with wind power in 2022, 25% of the region's total electricity generation for the year. ERCOT has also seen large investments in solar energy over the last 5 years; solar power electricity generation increased from 3.2 TWh in 2018 (0.8% of total generation) to 24.2 TWh in 2022 (5.6% of total generation). MISO produces far more wind power than solar power, with wind accounting for 14% of total generation in 2022 and only 1.2% attributed to solar power. CAISO produces comparatively much more solar power than ERCOT or MISO, with a total of 17% of it electricity coming from solar power. Wind power contributes 10.8% of CAISO's total power mix.

Wind power and solar power can have significant effects on the price of electricity. Large solar capacity depresses prices during the day when solar power is abundant before production tapers off in the evening hours as electricity demand peaks, with the severity of this effect depending on the weather and the season. The result is the ubiquitous "duck curve" in both net load and electricity price. Wind power is somewhat less predictable, with wind speeds constantly varying, though wind speeds tend to also follow roughly diurnal and seasonal trends. The varying levels of these renewable energy resources in each ISO contributes to the electricity price in each ISO having its own statistical characteristics.

The analysis in this paper is performed over annual periods using hourly data (8760 hours). However, a single year of data is insufficient for characterizing uncertainty in electricity price for a region due to the large, infrequent spikes in electricity price that may occur. This need for more data is balanced by the inherently changing market due to changes in generator installations (see the increase in ERCOT solar capacity, for example) and the availability of long-term historical data from these ISOs. With these considerations, data from 2018 to 2022 was collected for ERCOT and MISO, while the analysis for CAISO is limited to data from 2020 to 2022 due to the availability of complete historical data. Furthermore, the data from ERCOT for 2021 is omitted from this analysis. The severe winter storm in February 2021 that impacted Texas resulted in prolonged power outages and record-breaking electricity prices [17]. The mean electricity price in ERCOT in 2021 was over 2.5 times greater than in the year with the next highest mean because of this energy crisis, making 2021 a clear outlier in the ERCOT's historical price data. This data was initially included in this study, but early results indicated a greater than 200-fold increase in the revenue variance for the target IES design operating in ERCOT than when this data was omitted. A similar effect was not observed when removing any one year's data in the other ISOs studied here.

3 | CAPITAL COSTS AND OPERATING COSTS

Nuclear power plants are a capital-intensive investment, and there is significant uncertainty around capital costs for advanced nuclear reactors. Advanced nuclear reactor designs are at varying stages of development and have not yet seen widespread deployment, so estimates of advanced nuclear capital expenses (CAPEX) and operating expenses (OPEX) are used in lieu of costs from real-world projects for the purposes of this study. Recent reviews of advanced nuclear capital expenses (CAPEX) and operating expenses (OPEX), such as the works of Abou Jaoude et al. [12] and Stewart and Shirvan[13], have thoroughly addressed this topic. Readers are directed to these works for a more thorough review of the literature, but the references found therein that are used in this study are provided in Table 1 for completeness. This section synthesizes their results to build a distribution of advanced nuclear CAPEX and OPEX estimates. Estimates for TES costs are much more sparse in the literature, but these costs are expected to have less uncertainty than the nuclear costs and wholesale electricity revenue, so the TES uncertainties are treated less exhaustively. All monetary values given here are in 2022 USD ($\$_{2022}$). Estimates from other years are escalated to 2022 USD following the methodology of Ref. [12], which uses the 2017 edition of the Advanced Fuel Cycle Cost Basis

TABLE 1 Summary of cited works used for estimating uncertainty in NPP capital expenses and operating expenses, divided by reactor type

Cash Flow	PWR	HTGR	SFR	MSR
NPP CAPEX	[20] [21] [22] [23] [24] [25] [26] [27]	[20] [28] [27] [29]	[20] [30] [31] [13] [21] [32] [33] [34] [22] [35] [28]	[20] [27] [36] [37] [38] [39] [40]
NPP OPEX	[21] [26]	[28] [27]	[21] [32] [34] [41]	

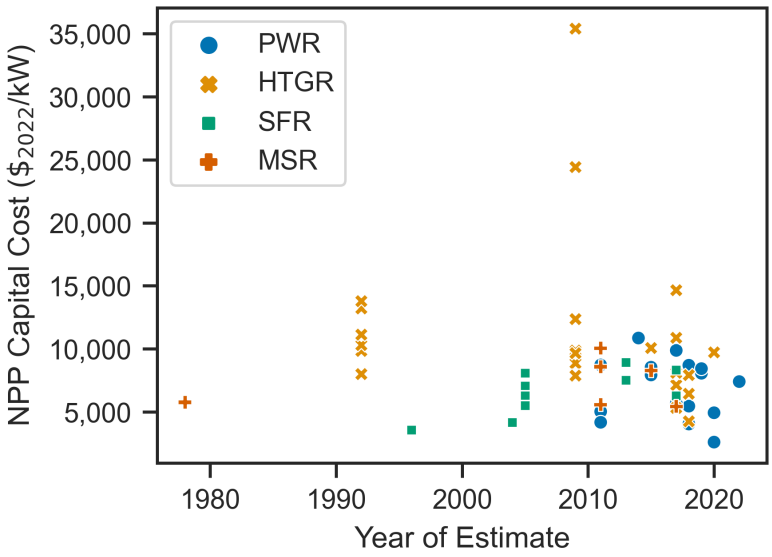

FIGURE 1 Escalated NPP CAPEX estimates with the year of the estimate and the type of reactor.

Report produced by Idaho National Laboratory (INL) [18] and the Producer Price Index for new industrial building construction from the U.S. Bureau of Labor Statistics [19] to derive escalation factors for each cost estimate by year.

A total of 56 estimates of NPP CAPEX from 22 studies are included in the distribution of values, given in units of $\$/kW_e$ of reactor capacity. These NPP CAPEX estimates include values given for pressurized water reactors (PWR), high temperature gas reactors (HTGR), sodium fast reactors (SFR), and molten salt reactors (MSR). There does not appear to be a significant difference in distribution of values by reactor type, so all reactor types are included in a single distribution here. As more detailed cost estimates are produced as advanced reactor designs come to maturity, this may no longer be the case. The escalated NPP CAPEX estimates are shown in Fig. 1, taken from the references in Table 1. There does not appear to be strong motivation to delineate these cost estimates by reactor type, given the significant overlap of their distributions and relatively few cost estimates for each reactor type individually. Therefore, the estimates from all four listed reactor types are considered as a single group. These estimates have a mean of $\$7900/kW_e$ and a standard deviation of $\$2600/kW_e$.

Only 11 estimates of NPP OPEX were found in the literature. After applying the same escalation procedure to these data, they have a mean of $\$34/MW_e$ and a standard deviation of $\$17/MW_e$. The escalated NPP OPEX estimates are plotted in Fig. 2, taken from the references in Table 1.

There is relatively little available data on costs for thermal energy storage systems. For capital costs, Mikkelson et al. [42] cite ranges of 5 to 30 $\$/kW_eh$ of energy capacity and 400 to 2100 $\$/kW_e$ for power costs, using the greater of the two for the system. For the system design of this study, which has a thermal capacity of 2.288 GW_th and the system's maximum power output of 500 MW_e, the power cost range produces the greater values. These costs are in line a similar TES system described in Knighton et al. [43], where a 500 MW_e system with 6 hours of thermal energy storage is estimated to have a power cost of 1272 $\$/kW_e$ using Hitec salt as the storage medium. Given that

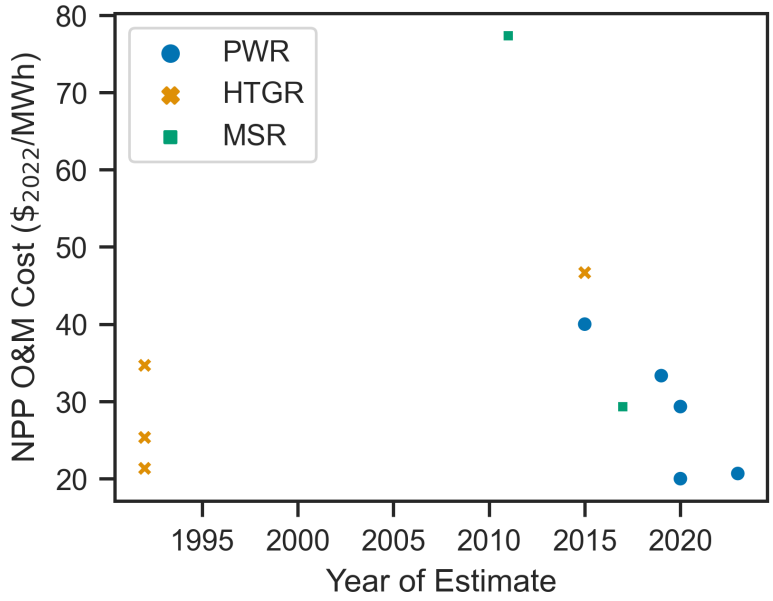

FIGURE 2 Escalated NPP OPEX estimates with the year of the estimate and the type of reactor.

only a simple range of costs is available rather than a distribution of cost estimates, we assume the upper and lower values of the range from Ref. [42] correspond to the upper and lower bounds of a uniform distribution to give equal probability to each value in the range, as was done previously by Hill et al. [16] in their related sensitivity analysis. Insufficient information about fixed and variable operating costs for TES systems was found in the literature, so these potential cost drivers are not included in this sensitivity analysis.

4 | SYSTEM MODEL

The nuclear power plant with integrated thermal energy storage is modeled using the Holistic Energy Resource Optimization Network (HERON) [44]. HERON is a tool for stochastic technoeconomic analysis of energy systems developed by the U.S. Department of Energy's Integrated Energy Systems program. In HERON, systems are modeled as high-level components that can produce, consume, or store a resource according to component capacities, dispatch requirements, and economic drivers. This is generally coupled to a stochastic time series model, created using the Risk Analysis Virtual Environment (RAVEN), to produce new time series realizations, or "synthetic histories," over which the system dispatch is optimized [45].

It has been noted previously in the literature that stochastic optimization of energy systems typically results in a different optimal design than systems optimized over only the historical data [46]. This stochastic approach to the technoeconomic analysis also allows for quantified uncertainty of cash flows dependent on these time series values, such as revenue from sales of electricity in a wholesale electricity market.

The energy system that is modeled is illustrated if Fig. 3. The NPP reactor provides heat to the system at a fixed rate of 834 MW_{th}. This heat is transferred to an intermediate storage loop with a two-tank thermal energy storage (TES) system with a capacity of 2.288 $GW_{th}h$. The working fluid of the storage loop is nominally a molten nitrate salt mixture (60% $NaNO_3$ and 40% KNO_3), though the modeling approach employed here is agnostic to the working fluids. Stored hot fluid can be drawn from the hot storage tank as needed to drive the electricity generation cycle of the balance of plant (BOP). The electricity produced by the BOP is supplied to the electricity grid, and the BOP electricity output is allowed to range between 200 MW_e and 500 MW_e. A fully-charged TES system is able to sustain the maximum 500 MW_e output for 5.5 hours before the electrical power output must be reduced and the storage recharged. Dana et al. [47] develop a detailed dynamic system model for this nuclear power plant plus thermal energy storage (NPP+TES) system using Dymola and the Modelica language. They observe BOP efficiencies

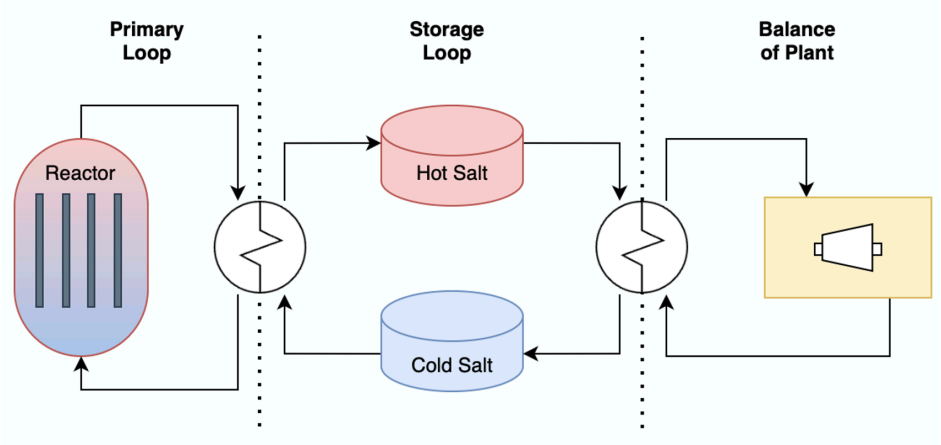

FIGURE 3 Illustration of a nuclear power plant with integrated thermal energy storage system. All heat produced by the nuclear reactor in the primary loop is transferred to the intermediate storage loop before being utilized by the balance of plant to generate electricity.

TABLE 2 System design parameters for the model of the nuclear power plant with thermal energy storage

Description	Variable	Value
Reactor thermal output	$\dot{W}_{reactor}$	834 MW_{th}
System electrical output	$\dot{W}$	200-500 MW_e
Steady operation electrical output	$\dot{W}_{steady}$	345 MW_e
Overall thermal efficiency	η	0.4
Power boosting max duration	τ	5.5 hours

ranging between 41.7% and 42.8%. Two-tank molten salt energy storage systems can have round-trip efficiencies of up to 93% [42]. The overall system efficiency is assumed to be a fixed 40%, which is roughly the product of these efficiencies. At 40% overall efficiency, the steady-state electrical output of the system is 345 MW_e. These model parameters are summarized in Table 2.

A numerical model can be constructed from the principles of conservation of mass and energy. For a fixed reactor output and approximately constant storage tank temperatures, the mass flow rate of storage fluid being drawn from the cold storage tank, passed through the primary loop heat exchanger, and deposited into the hot storage tank is a fixed rate; only the mass flow rate being drawn from the hot storage tank, or the equivalent electrical output, must be determined in an optimization. The power output is the only degree of freedom at each time step, so the system can be reduced to a single out-of-the-loop storage tank. To make this reduced model equivalent to the storage-in-the-loop design in Fig. 3, the BOP efficiency is taken to be the overall system efficiency (40%), while the thermal energy storage has no efficiency losses. While no real thermal energy storage system has a round-trip efficiency of 100%, this is mathematically equivalent to the two-tank storage model with non-unity round-trip efficiency.

The state of charge of the storage tank L at time t is defined to be

$$L(t) = L(0) + \sum_{s=1}^{t} \left(\dot{W}_{steady} - \dot{W}(t) \right), \tag{1}$$

where $\dot{W}_{steady}$ is the steady-state electrical output of the system, and $\dot{W}(t)$ is the electrical output of the system at time t. The outputs $\dot{W}(t)$ for $t = 1, \ldots, T$ are decision variables which are optimized to maximize revenue,

$$Revenue = \sum_{t=1}^{T} P(t)\dot{W}(t) \tag{2}$$

where $P(t)$ is the price of electricity at time t. The models used for electricity price will be described in greater detail in Section 5.2. The storage level is constrained to be periodic over time horizon $t \in [0, T]$,

$$L(0) = L(T), \tag{3}$$

and the storage level must not exceed the TES component capacity,

$$0 \leq L(t) \leq \tau \left(\dot{W}_{max} - \dot{W}_{steady} \right), \tag{4}$$

where τ is the time duration of storage while operating at maximum electrical output $\dot{W}_{max}$. The system outputs must fall within the minimum and maximum output bounds,

$$\dot{W}_{min} \leq \dot{W}(t) \leq \dot{W}_{max}, \tag{5}$$

with $\dot{W}_{min}$ = 200 $\mathrm{MW_e}$ and $\dot{W}_{max}$ = 500 $\mathrm{MW_e}$. This optimization problem for maximizing revenue subject to these constraints can be solved with linear programming methods. During this optimization of the system dispatch, price-taker assumptions are applied, meaning that the market is assumed to be large relative to the generation contributed by the system and that the electricity price is not effected by the system dispatch.

A time series of 8760 hourly electricity prices, totaling 1 year, is provided to the system model for each realization. Then, the system dispatch is solved over weekly (168 hour) windows. This window length was chosen because of the daily and weekly seasonalities observed in electricity price. Finally, cash flows are calculated over the 8760 hours of the optimized dispatch.

This study considers four uncertain cash flows: NPP CAPEX, NPP OPEX, TES CAPEX, and revenue. Each of these will be calculated on an annualized basis, with the system dispatch being solved over annual time periods. This is straightforward for cash flows which are already being calculated on an annual basis, like NPP OPEX and revenue. However, the up-front capital expenses must be annualized so that their respective uncertainties are not overly weighted compared to the recurring cost drivers.

The net present value (NPV) of a recurring cash flow can be expressed as

$$NPV = (1 - r_t) \sum_{y=0}^{N} \frac{\alpha \left(\frac{D_y}{D_{ref}} \right)^x}{[(1 + r_i)(1 + r_d))]^y}. \tag{6}$$

The numerator of the summed term is the cash flow equation, with reference cost α, cost driver D_y, reference driver D_{ref}, and x is a scaling factor. The contribution of the yearly cash flows are scaled by the tax rate r_t, interest rate r_i, and discount rate r_d. This study uses an inflation rate of 2.5%, tax rate of 25%, and a discount rate of 8%. Note that increases in the sum of inflation rate and discount rate will decrease the contribution of later years to the total NPV for the cash flow.

The NPV of a capital expense for a component with capacity C and reference cost α subject to amortization and depreciation is

$$NPV = \alpha C \left[1 - r_t \sum_{y=1}^{16} \frac{MACRS(y)}{[(1 + r_i)(1 + r_d))]^y} \right]. \tag{7}$$

The 15-year MACRS schedule, the modified accelerated cost recovery system, is used to calculate depreciation. To annualize this NPV, the expression in Eq. 7 can be equated to a single recurring cash flow like in Eq. 6 to find the equivalent reference cost α_{equiv} for a recurring cash flow over the life of the component, N_{life}. This equivalent reference cost is then

$$\alpha_{equiv} = \alpha \frac{1 - r_t \sum_{y=1}^{16} \frac{MACRS(y)}{[(1+r_i)(1+r_d))]^y}}{\sum_{y=1}^{N_{life}} \frac{1}{(1+r_d)^y}}. \tag{8}$$

The lifetime of the nuclear reactor is assumed to be 60 years, and the life of the thermal energy storage and balance of plant components is assumed to be 30 years. Applying Eq. 8 to these lifetimes yields capital recovery factors of 0.0888 and 0.0808 for 30- and 60-year lifetimes, respectively.

Finally, the total system NPV (NPV_{tot}) is simply the sum of the NPV of each of the aforementioned cash flows:

$$NPV_{tot} = NPV_{npp,capex} + NPV_{npp,opex} + NPV_{tes,capex} + NPV_{revenue}. \tag{9}$$

5 | UNCERTAINTY QUANTIFICATION METHODS

The uncertainty in the NPP CAPEX, NPP OPEX, and TES CAPEX cash flows can be reduced to uncertainty in the reference costs α. For the revenue cash flow, however, there is uncertainty in both the reference cost α and the cost driver D_y, which is the dispatch of the system, because both variables are dependent on the stochastic time series of electricity price. This section describes the methods used for quantifying the contributions to uncertainty in NPV_{tot} from each of these sources of uncertainty.

5.1 | Sobol Indices

Sensitivity analysis seeks to attribute variance in a model output to variance in model inputs. Sobol indices provide a convenient, normalized form to compare the variance contributions from each source of uncertainty [48]. This is done through variance decomposition. For our model, calculating the Sobol indices for the uncertain input parameters for each ISO will quantify the sensitivity to each uncertainty source for each market.

Sobol indices are defined by the ratio of variance in a function Y attributable to some combination of uncertain inputs $X_1, X_2, \ldots, X_d$ to the total variance in Y. For an individual input X_i, its Sobol index S_i is

$$S_i = \frac{Var(E(Y|X_i))}{Var(Y)}. \tag{10}$$

Sobol indices for individual inputs are known as first order indices. The Sobol index for two inputs together, X_i and X_j, is defined as

$$S_{ij} = \frac{Var(E(Y|X_i, X_j)) - Var(E(Y|X_i)) - Var(E(Y|X_j))}{Var(Y)}. \tag{11}$$

Known as second order indices, Sobol indices of two inputs quantify the variance contribution of the interaction of X_i and X_j beyond their individual variance contributions. This process can be continued for all subsets of u. More generally, for some arbitrary combination of uncertain inputs $X_1, X_2, \ldots, X_d$, denoted by X_u where $u \subset \{1, 2, \ldots, d\}$, the Sobol index S_u is

$$S_u = \frac{Var(E(Y|X_u)) - \sum_{v \in V} Var(E(Y|X_v))}{Var(Y)}, \quad u \subseteq \{1, 2, \ldots, d\},\ V = \mathcal{P}(u) - \{u\}, \tag{12}$$

where $V = \mathcal{P}(u) - \{u\}$ is the set of all subsets of u (the power set of u) minus u itself. The first term in the numerator is the total variance contributed to Y by the inputs in X_u, and the second term in the numerator removes the contribution of lower-order combinations. To make this notation more concrete, take $u = \{1, 2\}$ as an example. Then, $X_u = \{X_1, X_2\}$ and $V = \{\{1\}, \{2\}\}$. Applying this to Eq. 12, the expression becomes

$$S_{12} = \frac{Var(E(Y|X_1, X_2)) - [Var(E(Y|X_1)) + Var(E(Y|X_2))]}{Var(Y)}, \tag{13}$$

which recovers the expression from Eq. 11.

The total sensitivity to some parameter X_i can be summarized in the total sensitivity index S_{T_i}. This total sensitivity index is the sum of all indices , which is defined as

$$S_{T_i} = 1 - \frac{Var(E(Y|X_{\sim i}))}{Var(Y)}, \tag{14}$$

where the notation $X_{\sim i}$ indicates the set of all inputs except X_i. The total sensitivity index includes variance from the parameter itself and all of its higher-order interactions.

Calculating Sobol indices often comes at significant computational expense when $Var(E(Y|X_u))$ must be estimated numerically through Monte Carlo sampling. For $Y = NPV_{tot}$, however, the considered sources of uncertainty contribute to variance in NPV_{tot} independently and in a strictly additive fashion. This significantly simplifies the calculation of the Sobol indices. The remainder of this section focuses on the derivation of expressions for calculating some Sobol indices of NPV_{tot} analytically.

Beginning with the denominator in Eq. 12,

$$\begin{aligned} Var\left(NPV_{tot}\right) &= Var(NPV_{npp,capex} + NPV_{npp,opex} \\ &\quad + NPV_{tes,capex} + NPV_{revenue}) \end{aligned} \tag{15}$$

$$\begin{aligned} &= Var\left(NPV_{npp,capex}\right) + Var\left(NPV_{npp,opex}\right) \\ &\quad + Var\left(NPV_{tes,capex}\right) + Var\left(NPV_{revenue}\right), \end{aligned} \tag{16}$$

since the random variables on which each component NPV depends are independent of each other. Therefore, the variance of each cash flow can be calculated individually. Taking the variance of Eq. 6 gives the general form of this variance term:

$$Var(NPV) = Var\left((1-r_t)\sum_{y=0}^{N}\frac{\alpha\left(\frac{D_y}{D_{ref}}\right)^x}{[(1+r_i)(1+r_d))]^y}\right). \tag{17}$$

For the CAPEX and OPEX cash flows, this reduces to

$$Var(NPV) = \left((1-r_t)\sum_{y=0}^{N}\frac{\alpha\left(\frac{D_y}{D_{ref}}\right)^x}{[(1+r_i)(1+r_d))]^y}\right)^2 Var(\alpha) \tag{18}$$

since only α is uncertain. While it is immediately apparent that all of the other terms in the equation are constants for the CAPEX cash flow, the cost driver D_y in the OPEX cash flow is the total electricity produced in year y and is therefore a function of the system dispatch. However, since the heat output of the NPP is held constant, all heat produced must eventually be converted to electricity, and the heat stored in the TES system must be equal at times $t = 0$ and $t = 8760$ (the end of the year), the total electricity produced must be equal to the total heat produced times the efficiency of the balance of plant, making D_y a constant in this case as well. The variance of α can then be calculated using the distribution of estimates from Section 3.

The expression for $Var(NPV_{revenue})$ does not reduce so nicely due to the dependence of both D_y and α on the price time series P_t. This term must be calculated numerically through Monte Carlo sampling of P_t. The following two subsections describe the sampling methods that are applied when estimating this term.

With the individual NPV variances having been calculated, the numerator of Eq. 12 is trivial to calculate. The uncertainties in NPV_{tot} are additive, so

$$Var(E(NPV_{tot}|X_i)) = Var(NPV_i), \tag{19}$$

which has just been calculated for each cash flow NPV_i. Finally, returning to Eq. 12 with three terms of the form of Eq. 18 for the NPP CAPEX, NPP OPEX, and TES CAPEX cash flows, and one term of the form of Eq. 17 for the system revenue,

$$S_i = \frac{Var(NPV_i)}{\sum_{j=1}^{4} Var(NPV_j)},\ i \in \{1,2,3,4\}. \tag{20}$$

Only $Var(NPV_{revenue})$ must be estimated numerically to calculate all of the Sobol indices. Furthermore, it can be seen here that the 4 first-order Sobol indices of NPV_{tot} account for all of the variance in NPV_{tot}. All of the second-order and higher indices are zero, and the total Sobol indices from Eq. 14 and the first-order indices are equivalent.

5.2 | Stochastic Time Series Model

One method for estimating the uncertainty in NPV_{tot} due to the price time series P_t is to fit a stochastic model to P_t and solve the dispatch problem from each realization. This Monte Carlo approach using scenario generation has been used by a number of studies in the past, such as those in references [49, 50, 14]. In this study, we apply a vector ARMA (VARMA) model to the data to take advantage of correlations among price, load, wind, and solar data when generating synthetic price time series [51].

The data must be detrended and normalized before fitting a VARMA model. The major tends to be removed are periodic trends, such as diurnal and annual trends in electricity load. Chen and Rabiti [52] propose removing these periodicities by subtracting corresponding Fourier modes from the signal then applying a gaussianizing transformation to the residual. For the data used in this study, it was found to be beneficial to include additional data transformations. The following procedure was applied to the historical data segmented into approximately monthly segments of 730 hours, in line with the detrending procedures of previous studies, e.g. [53, 54].

First, significant year-to-year trends in the data are removed. These long-term trends are removed from the wind and solar data ($X_{t,wind}$ and $X_{t,solar}$, respectively) by normalizing the total installed capacity C for each resource and region,

$$R_{t,wind} = \frac{X_{t,wind}}{C_{wind}(t)}, \tag{21}$$

$$R_{t,solar} = \frac{X_{t,solar}}{C_{solar}(t)}. \tag{22}$$

This results in a capacity factor that ranges between 0 and 1 at each time t. The price and total load series are detrended by subtracting the median value and scaling by the interquartile range,

$$R_{t,load} = \frac{X_{t,load} - med(X_{load})}{IQR(X_{load})}. \tag{23}$$

The price time series residuals are further transformed with a hyperbolic arcsine function, a log-like function that accepts both positive and negative values, to reduce the severity of price spikes before passing the residual series on to subsequent modeling steps [55],

$$R_{t,price} = \operatorname{arcsinh}\left(\frac{X_{t,price} - med(X_{price})}{IQR(X_{price})}\right). \tag{24}$$

Then, the significant Fourier modes of the residual are removed, where the periods of these modes (p_i) are manually specified, though their The total Fourier signal removed from residual R_t is

$$F_t = \sum_{i=1}^{M} A_i \sin\left(\frac{2\pi t}{p_i}\right) + B_i \cos\left(\frac{2\pi t}{p_i}\right), \tag{25}$$

where the coefficients A_i and B_i are determined through least squares regression. This Fourier signal removal is applied to all variables except solar power. During the nighttime hours, solar power generation is exactly zero, making applying such a Fourier detrending algorithm to the series difficult. This is remedied somewhat by masking the zero values, fitting the Fourier signal to the non-zero values, then replacing the zeros in the synthetic signal to ensure that the nighttime periods are correctly preserved. While this method does preserve the nighttime values well, it tended to produce anomalous values in the morning and evening hours. A better reproduction of the solar power series in these morning and evening hours is achieved by using an STL decomposition, which decomposes the signal into trend, seasonal, and residual components [56]. In the case of solar power, a periodicity of 24 hours is specified for the STL decomposition, and the sum of the trend and seasonal components sum to be the total mean trend for the solar power data,

$$F_{t,solar} = S_{t,solar} + T_{t,solar}, \tag{26}$$

where S_t and T_t are those seasonal and trend components, respectively, as calculated from the STL decomposition of $R_{t,solar}$. Finally, the resulting signal is gaussianized through a probability integral transformation [57, 52]

$$N_t = \Phi^{-1}\left[f\left(R_t - F_t\right)\right], \tag{27}$$

where Φ is the cumulative distribution function (CDF) of the standard normal distribution and f is the CDF of the residual signal $R_t - F_t$. The CDF of the residual is not known, so it is estimated through kernel density estimation. The normalized signal N_t should now be sufficiently stationary to fit a VARMA model, defined by

$$Y_t = \mu + \sum_{i=1}^{P} \phi_i Y_{t-1} + \sum_{j=1}^{Q} \theta_j Y_{t-1} + \varepsilon_t, \tag{28}$$

where Y_t are vectors of k variables, P and Q are the autoregressive and moving average orders, respectively, μ is a constant, ϕ_i and θ_j are each $k \times k$ matrices, and ε_t is a noise term of distribution $\mathcal{N}(0, \sigma^2)$. A VARMA model with $P = 2$ and $Q = 3$ is used for this study.

A separate model is fit to each month of the multi-year series of historical data for each region. While the detrending steps outlined above target removing trends in the mean of the signal, they do nothing to address changes in autocorrelative and cross-correlative behavior. These do not appear to change significantly over short timescales, and fitting a model to each month-long segments is sufficient for negating stationarity concerns over longer time frames.

To generate a time series of one year in length, a model for each month is randomly drawn from the models for that month from each year of available data. Then, a noise signal is generated using the VARMA model, and the transformation of Eq. 27 is inverted, followed by the adding the Fourier signal back in and inverting the remaining transformations and scalings. When generating a signal, the robust scaling step, as in Eq. 23, the median and interquartile range from the 2022 series are used. This is to ensure that the resulting synthetic time series for price is in 2022 USD.

Figure 4 shows the distribution of historical price data compared to that of 100 samples generated using the fitted models. The values of each series are scaled using Eq. 24 to facilitate the visualization by reducing the severity of the right-tail values relative to the rest of the distribution. Visually, it can be seen that the historical and sampled distributions are similar but not exactly the same. The differences between them tend to be most pronounced at the tails of the distributions, with the distributions generally matching well in the high-density portions of the probability distributions. It is desired that the samples be statistically similar to the historical data, but one of the benefits of using a time series modeling approach such as this is that the model may generate values beyond the bounds of the historical data. In the judgement of the authors here, these models fit the data sufficiently well for the purposes of this study. However, this is an area of potential improvement, particularly with respect to the correct estimation of the frequency, magnitude, and duration of extreme price spikes.

5.3 | The Block Bootstrap

Another approach to the time series uncertainty quantification problem is to employ a block bootstrap resampling method. Bootstrapping entails random sampling with replacement from a collection of samples to estimate the properties, such as the variance, of some measure of the samples [58]. While the bootstrap is a powerful tool, it requires that the samples of the data be independent, and autocorrelated time series values are not independent. Block bootstrap methods were introduced to address this case of bootstrapping with autocorrelated signals [59].

The block bootstrap accommodates an autocorrelated signal by resampling blocks of sequential samples with replacement, assembling these blocks into a bootstrap pseudo-series, then estimating the property of interest from that resulting pseudo-series. In this study, the circular block bootstrap of Politis and Romano [60] is used. The sampling method for the circular block bootstrap is depicted in Fig. 5. Starting with a series of observations $X_1, \ldots X_n$, the procedure for estimating some property θ, where its bootstrap estimate is denoted $\hat{\theta}_n$, using the circular block bootstrap is as follows [61]:

1. Resample with replacement $k = \lceil n/b \rceil$ blocks of observations of length b from the observations $X_1, \ldots, X_n$. This is done with the observations "wrapped" in a circle, where blocks may begin near the end of the series and wrap

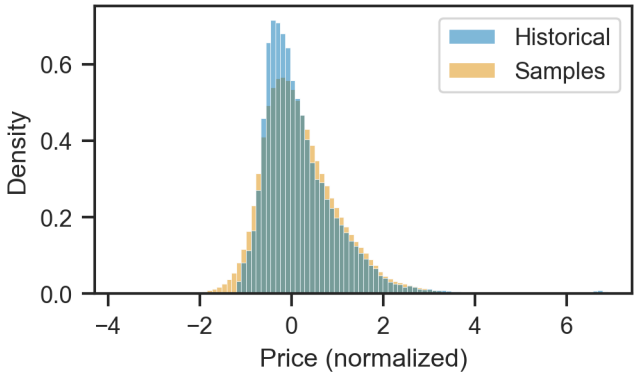

(a) ERCOT

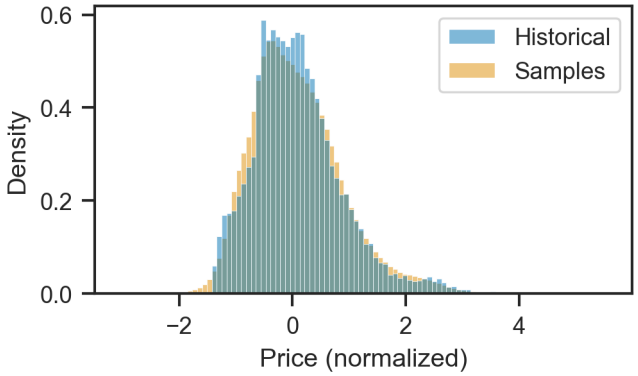

(b) CAISO

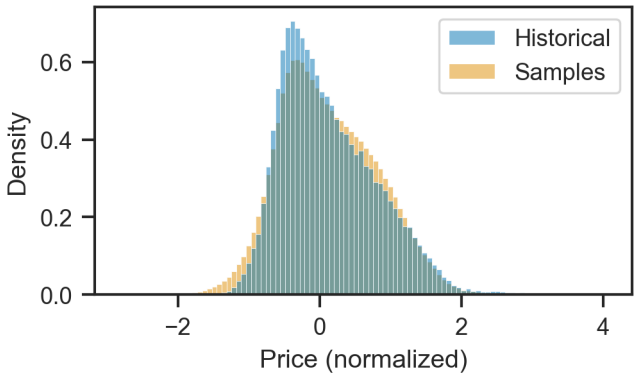

(c) MISO

FIGURE 4 A comparison of the distributions of the historical price data and 100 samples of the time series model for (a) ERCOT, (b) CAISO, and (c) MISO. Both series are normalized with Eq. 24 to facilitate the visualization.

around to the beginning of the series; this is the defining feature of the circular block bootstrap (see Fig. 5). Resampling blocks in this way results in more equitable usage of observations near the beginning and end of the series.

2. Concatenate these k blocks to form the bootstrap pseudo-series

$$X_1^*, \ldots, X_b^*, X_{b+1}^*, \ldots, X_{2b}^*, \ldots, X_{n-b+1}^*, \ldots, X_n^*.$$

The superscript $*$ indicates a bootstrapped quantity. If n/b is not an integer, keep only the first n observations from the pseudo-series.

3. Repeat M times to generate M bootstrap pseudo-series.
4. For each pseudo-series $j = 1, \ldots, M$, calculate the sample statistic $\hat{\theta}_n^{*(j)}$.
5. The mean of $\hat{\theta}_n^*$ is

$$\mathbb{E}^* \left[\hat{\theta}_n^* \right] = \frac{1}{M} \sum_{j=1}^{M} \hat{\theta}_n^{*(j)}, \tag{29}$$

and its variance is

$$\mathrm{Var}^* \left(\hat{\theta}_n^* \right) = \frac{1}{M} \sum_{j=1}^{M} \left(\hat{\theta}_n^{*(j)} - \mathbb{E}^* \left[\hat{\theta}_n^* \right] \right)^2. \tag{30}$$

This procedure still requires the selection of block length b. The optimal block length is the block length which maximizes the convergence rate of the bootstrap estimate. Blocks that are too short will not contain enough data to capture the autocorrelative behavior of the signal, and the estimates of θ for each block will not be independent of each other. Blocks that are too long will produce independent estimates of θ but will not make efficient use of the available data, limiting the convergence rate of the bootstrap estimand. The block length selector of Politis and White [62] uses the sample autocorrelation function to estimate this optimal block length. This block length selector is used to choose the block length for each series here.

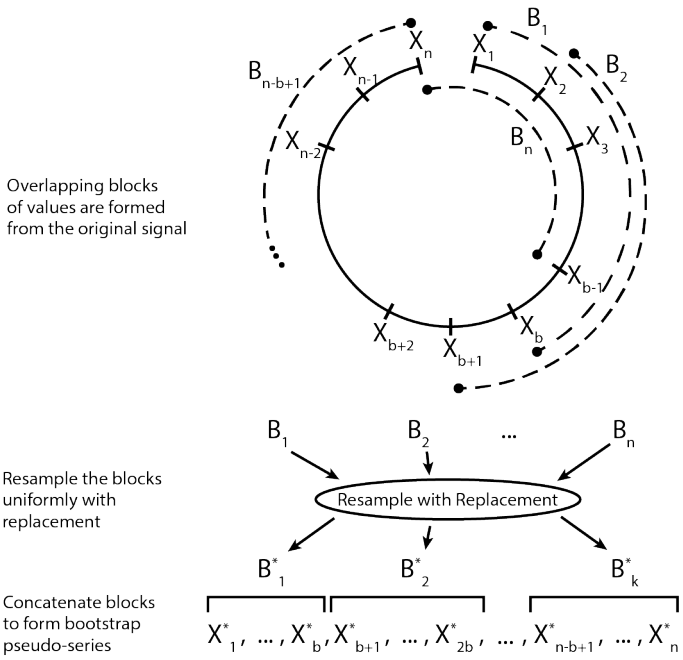

FIGURE 5 The sampling methodology for the circular block bootstrap allows blocks to wrap from the end of the series to the beginning of the series to more efficiently use data near the ends of the series.

Taking $\hat{\theta}_n = \sum_{i=1}^{n} X_i$ to be the quantity of interest and using data for the hourly revenue of the IES over a period of time, it is possible to estimate the total revenue of the system over the period of time between X_1 and X_n with quantified uncertainty. The hourly system revenue is just a product of the hourly electricity price P_t and the hourly electricity dispatched to the grid D_t. The observed signal must be stationary to apply the circular block bootstrap method. The dispatch quantity D_t can reasonably be assumed to be stationary since the capacity of the system is not changing over time, but the electricity price is not stationary and requires detrending before the circular block

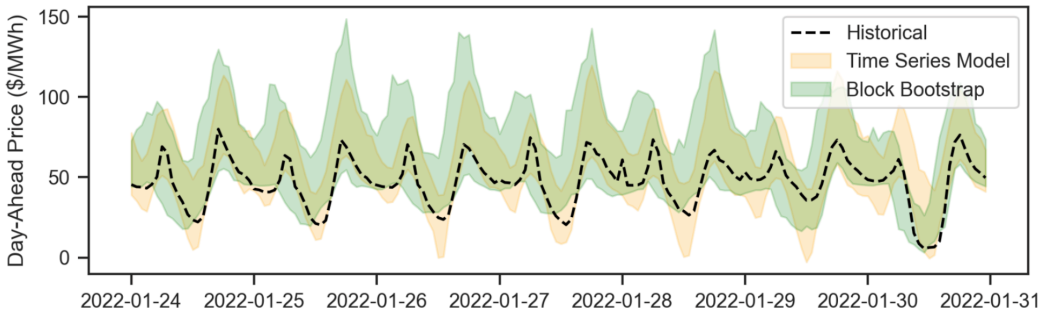

FIGURE 6 One week of historical price data from CAISO from January 2022 with 95% confidence bounds for the series generated by each time series sampling methodology, calculated from 100 samples

bootstrap can be applied. Since the block bootstrap makes no assumptions about the distribution of the observations, a more simplified detrending procedure can be applied to the electricity price than was applied in Section 5.2. Only the long-term trends are removed from the signal by applying the scaling transformation of Eq. 23, while the daily-scale trends are left in tact. Requiring that the block length be at least 24 hours ensures that the these daily seasonalities are left intact in the bootstrap pseudo-series. After constructing the pseudo-series, the long-term trends are added back in to the series.

There are several advantages to using a block bootstrap method instead of sampling from a time series model in some situations. Block bootstrap methods are model-free uncertainty quantification methods, meaning that no assumptions about the distribution of values or the autocorrelation structure of the data are made when applying these methods. The modeling assumptions that are made when fitting a time series model, like the VARMA model described in the previous section, can be limiting when the autocorrelation function may not be well-described by finitely-many autoregressive or moving average terms. Additional detrending or normalization steps are also often required for many time series models to be applicable, such as the gaussianizing transformation in Eq. 27. Furthermore, estimating the uncertainty in system revenue using the VARMA model described earlier requires extensive sampling, with each time series sample requiring the computationally expensive dispatch optimization problem to be solved. Using the bootstrap method, the dispatch problem must be solved only for the historical price data, reducing computational expense by around two orders of magnitude. However, bootstrap methods do impose some limitations on the analyses that can be conducted. Bootstrap methods are, by definition, limited to using historical observations. The range of extreme events is limited to those previously observed. The electricity market that is being modeled is essentially frozen in time, being restricted to the market conditions which produced the historical data. Time series modeling approaches are more flexible and can incorporate our knowledge of the physical processes and market behaviors which produced the historical data to analyze evolving markets. Given the computational savings of the bootstrapping approach, demonstrating its usage in this type of analysis is a valuable contribution, though its limitations should be kept in mind when comparing these two methodologies.

6 | RESULTS & DISCUSSION

The two time series sampling methodologies produce similar time series. The block bootstrap is applied directly to the time series of hourly revenue, which is a function of the historical price time series, while the VARMA model is used to first generate synthetic time series data for price before the system dispatch is optimized over each sample. For the purposes of comparing the two methods, the samples shown are both of electricity price. Figure 6 plots one week of CAISO historical price data from 2022 along with 95% confidence bounds of 100 samples from each time series method. The range of samples from each method matches the daily seasonalities in the historical data well. Over this particular date range, the bootstrap samples appear to have greater variance than the time series model, though this is not necessarily the case over year-long realizations.

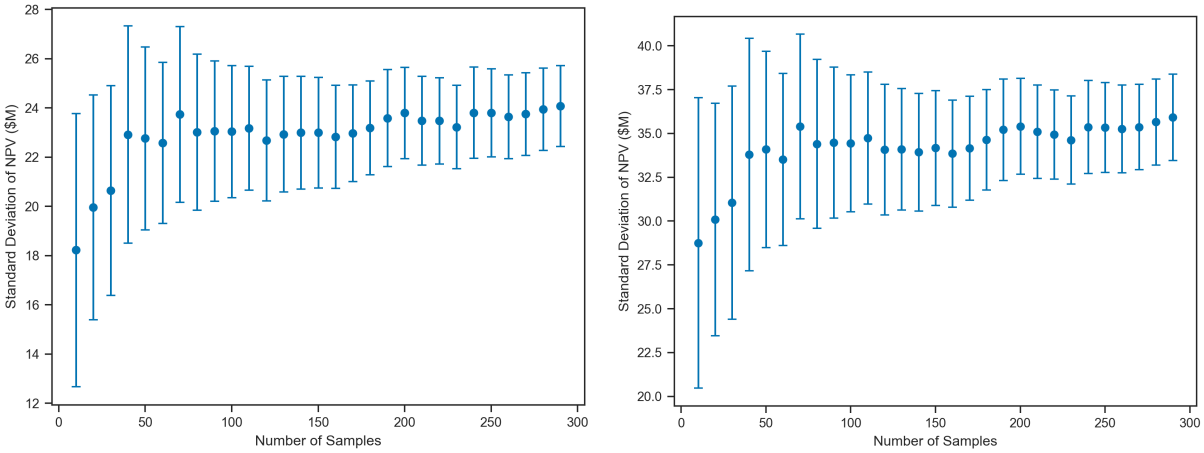

(a) Baseline Case (b) TES Case

FIGURE 7 Convergence of standard deviation (equivalent to convergence in variance) for revenue for ERCOT using the time series model sampling method for (a) the baseline design (no TES) and (b) the design with TES.

The distribution of revenue for each ISO is estimated using sampling of the time series model and block bootstrapping with the historical price data from each ISO. In the time series modeling approach, the estimate of the revenue variance stabilizes after approximately 100 samples, so 100 samples are used in each case. Variance estimates using up to 300 samples for ERCOT, both for the baseline system and the system with TES, are shown in Fig. 7, including bootstrapped 95% confidence intervals about each estimate. In both cases, the variance estimate stabilizes in fewer than 100 samples, though the confidence bounds continue to decrease with the square root of the number of samples. The block bootstrap uses 1000 resampled series to estimate the distribution of revenue. It is possible to use an order of magnitude more samples with the block bootstrap than the model-basd approach because of the reduced computational expense associated with the method.

Figures 8-10 compare the distribution of annual revenues between the time series (blue) and bootstrap methods (orange) across ISOs. The dashed vertical lines mark the revenue calculated from each year of the historical price data used, the mean of which is recorded with the solid vertical line. From the distributions plotted, it can be seen that the distributions of revenue from both methods are reasonably similar for CAISO and MISO: the location and scale of the distributions are similar. However, there is a large discrepancy in the two methods' distributions for ERCOT. This seems to be caused by the bootstrap method being capable of including price spikes from multiple past years in a single year's bootstrap series, causing a strengthening of the distribution's right tail. In fact, this discrepancy highlights a limitation of the available data. ERCOT's historical price data is quite "spiky" relative to the other two ISOs discussed here, with price spikes far exceeding the magnitude of those seen in the other ISOs. Given limited historical data, it can be difficult to accurately model those extreme, infrequent spikes using any data-driven methodology. Additional modeling relying on knowledge of the mechanics of price formulation in deregulated electricity markets would be warranted for better characterizing the tails of the distribution.

The importance of variance in revenue relative to the other cost uncertainties that have been modeled can be summarized in Sobol indices for each ISO. The mean of the estimates of variance of $NPV_{revenue}$ from the time series sampling method and block bootstrap method is used for the variance of $NPV_{revenue}$ when calculating the Sobol indices. The Sobol indices for each ISO are plotted in Fig. 11.

The variance in the NPP CAPEX, NPP OPEX, and TES CAPEX cash flows are constant across ISOs, but the normalization by the total uncertainty in NPV_{tot} causes the Sobol indices for these costs to vary among regions. In all cases, the uncertainty in NPP CAPEX is the dominant uncertainty, followed by NPP OPEX. Uncertainty in TES CAPEX, even assuming a relatively significant amount of uncertainty relative to the mean of that cash flow, is largely unimportant. There is significant variance in how significantly the revenue uncertainty is across ISOs. In ERCOT, revenue uncertainty accounted for 18.5% of the total variance in NPV_{tot} but only 7.1% in CAISO and 2.0% in MISO. In MISO, revenue uncertainty is the least significant source of uncertainty of the sources considered.

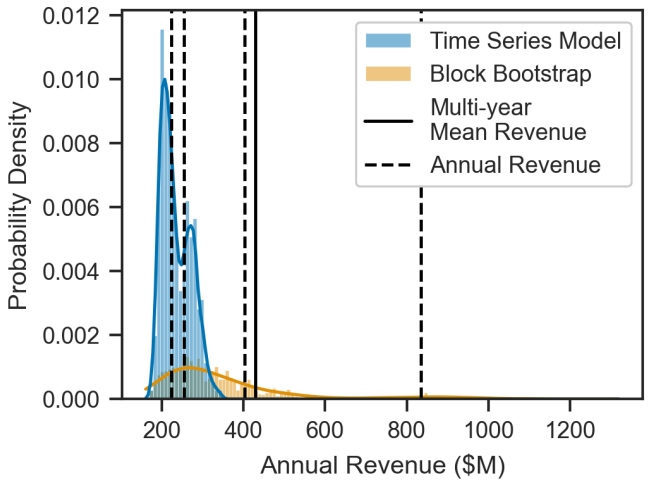

FIGURE 8 Distribution of annual system revenue estimated using the time series model and block bootstrap method for ERCOT

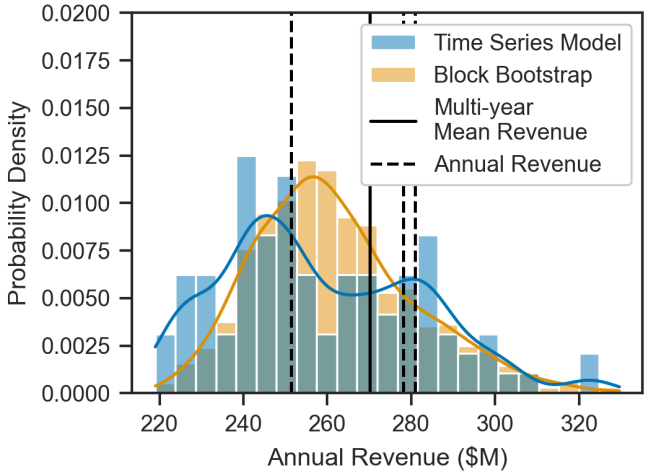

FIGURE 9 Distribution of annual system revenue estimated using the time series model and block bootstrap method for CAISO

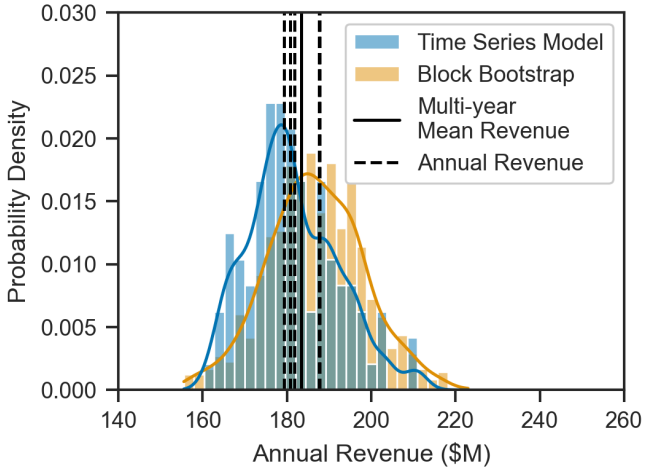

FIGURE 10 Distribution of annual system revenue estimated using the time series model and block bootstrap method for MISO

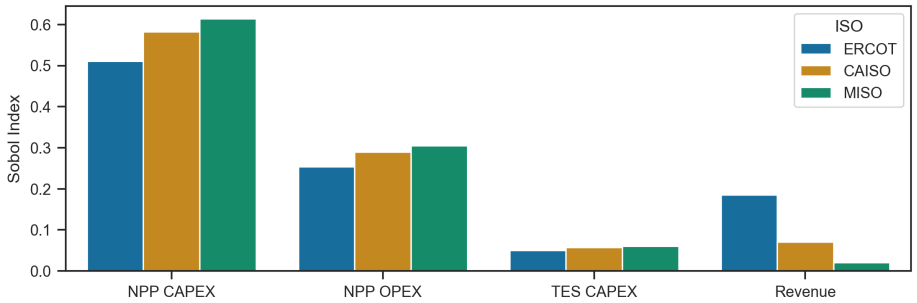

FIGURE 11 Sobol indices for variance in total system NPV due to variance in NPP CAPEX, NPP OPEX, TES CAPEX, and revenue

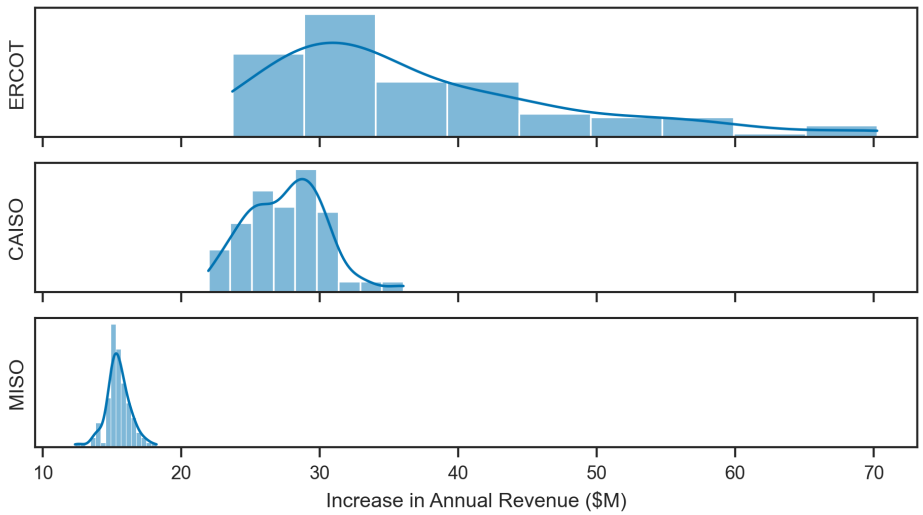

FIGURE 12 Distributions of increase in annual revenue due to the use of a thermal energy storage system

Adding a TES component to the system design has the effect of increasing sensitivity to the price time series uncertainty. This is observed by repeating the sensitivity analysis with an equivalently-sized nuclear reactor that operates at a constant electrical output. This also follows quite directly from the dispatch optimization. The system that includes a TES component sells more electricity during high price periods and less electricity during low price periods compared to the constant dispatch system. For a given price time series, this dispatch strategy increases the high values of the revenue time series while also decreasing its low values; this is an increase in variance. Both designs are evaluated over the same set of 100 synthetic histories so the direct effect of adding a TES component to the system can be observed. The distribution of increase in revenue from adding the TES for each ISO is shown in Fig. 12.

One immediately apparent effect of adding the TES system is the increase in revenue seen in every ISO due to the system dispatch policy being able to favor high price periods. The mean annual revenue increased by $37.3M in ERCOT, $27.6M in CAISO, and $15.4M in MISO. Comparing the spread of the distributions, the standard deviation of the revenue distribution increased by $10.8M in ERCOT, $2.5M in CAISO, and $0.6M in MISO. In summary, all ISOs saw in increase in both the mean and variance of the revenue distribution with the addition of TES to the system design, but the degree of this effect was most pronounced in ERCOT.

Finally, one obvious question remains when comparing these cases: does the increased revenue exceed the cost of the TES system? For the assumed discount rate and inflation rate, the distribution of total TES CAPEX values for the system form a uniform distribution between $16M and $82M. Returning to Fig. 12, it can be seen that the

distribution of revenue increase falls entirely within this range for ERCOT and CAISO, and the distribution for MISO lies about the lower bound of that range. Therefore, this system design may not be appropriate for the MISO market. However, the system design has not been optimized for each market in this study, and this may not be the case for all system configurations.

7 | CONCLUSIONS

A nuclear hybrid energy system consisting of a nuclear power plant (NPP) and a thermal energy storage (TES) system is modeled in three US deregulated electricity markets. The uncertainties in NPP capital and operating expenses, TES capital expenses, and revenue generated by selling electricity in the day-ahead electricity market are quantified. A block bootstrap approach for quantifying uncertainty in the electricity price and its effect on plant revenue is introduced and provides an approximately 100-fold reduction in computation time compared to the ARMA-based Monte Carlo methodology used in previous studies. This block bootstrap approach also makes no assumptions about the distribution of data or its autocorrelation function, which are limiting assumptions of the ARMA-based models. In addition, the distribution of annual revenue estimated by the block bootstrap method for ERCOT appear to better fit the annual revenue calculated for the historical data over the years collected, indicating that the time series model may have been unable to adequately model the price spikes in the extreme right tail of the distribution of electricity price which contribute significantly to overall plant economics.

Across all three ISOs considered, NPP capital expenses are the leading source of uncertainty in total system NPV, followed by NPP operating expenses. Between 2.0% (MISO) and 18.5% (ERCOT) of the total NPV variance is attributed to uncertainty in revenue. The uncertainty in TES capital costs contributes only 4-5% of the overall variance. For markets with minimal uncertainty contribution from revenue, it may not be worthwhile to model in great detail. However, in regions such as ERCOT, it is a significant source of uncertainty and should be included in techno-economic analyses if the uncertainty in NPV is to be adequately quantified. While this revenue uncertainty may not be the leading source of uncertainty for new-build advanced nuclear plants, it is an uncertainty source that will exist for the generator across its lifetime but change over time, as well, as renewable energy penetration increases, existing fossil fuel electricity generators are retired, and broad electrification across economic sectors continues. Future analyses considering greater penetration of wind, solar, nuclear, and other low-emission energy sources in deregulated electricity markets may be able to show how significant this uncertainty will change as the electricity generation infrastructure is decarbonized to meet national emissions goals.

Every regional electricity market has its own characteristics. This study considered only three US markets. Extending this sensitivity analysis to other competitive foreign and domestic markets would benefit the robustness of the conclusions drawn here and would be beneficial for guiding deployment of advanced reactor systems in diverse markets. Additionally, the sensitivities calculated here are a function of the optimal system dispatch and therefore the system design, so extending this analysis to additional designs, especially those with a greater diversification of end-use energy products, is of great interest for further study.

ACKNOWLEDGMENTS

The authors are grateful for the financial support of the U.S. Department of Energy Nuclear Energy University Program (award number DE-NE0009159).

DECLARATION OF COMPETING INTERESTS

The authors declare that they have no known competing financial interests or personal relationships that could have appeared to influence the work reported in this paper.

DATA AVAILABILITY STATEMENT

The data that support the findings of this study are available from the corresponding author upon reasonable request.

CREDIT

Jacob A. Bryan: Conceptualization, Methodology, Software, Formal Analysis, Investigation, Writing - Original Draft, Visualization. **Hailei Wang**: Writing - Review & Editing, Supervision, Project Administration, Funding Acquisition. **Paul W. Talbot**: Conceptualization, Writing - Review & Editing, Supervision, Project Administration

REFERENCES

1. The White House, (2021).
2. Paul Denholm, Patrick Brown, Wesley Cole, Trieu Mai, Brian Sergi, Maxwell Brown, Paige Jadun, Jonathan Ho, Jack Mayernik, Colin McMillan, Ragini Sreenath, NREL/TP-6A40-81644, 1885591, MainId:82417 (2022). https://www.osti.gov/servlets/purl/1885591/.
3. A. Epiney, C. Rabiti, P. Talbot, A. Alfonsi, Applied Energy **260**, 114227 (2020).
4. Rodica Loisel, Victoria Alexeeva, Andreas Zucker, David Shropshire, Progress in Nuclear Energy **109**, 280 (2018).
5. Shannon Bragg-Sitton, Cristian Rabiti, Richard Boardman, James O'Brien, Terry Morton, SuJong Yoon, Jun Yoo, Konor Frick, Piyush Sabharwall, T. Harrison, M. Greenwood, Richard Vilim, INL/EXT–20-57708-Rev.01, 1670434 (2020). https://www.osti.gov/servlets/purl/1670434/.
6. Giorgio Locatelli, Andrea Fiordaliso, Sara Boarin, Marco E. Ricotti, Progress in Nuclear Energy **97**, 153 (2017).
7. Roxanne Pinsky, Piyush Sabharwall, Jeremy Hartvigsen, James O'Brien, Progress in Nuclear Energy **123**, 103317 (2020).
8. Charles W. Forsberg, Nuclear Technology **206**(11), 1659 (2020), Publisher: Taylor & Francis _eprint: https://doi.org/10.1080/00295450.2020.1743628.
9. TerraPower, *Demonstrating the Natrium Reactor and Integrated Energy System: Cost-Competitive, Flexible Technology for the Clean Energy Future* (2023). https://www.terrapower.com/wp-content/uploads/2023/03/TP{_}2023{_}Natrium{_}Technology-0215.pdf.
10. Paul Joskow, Jean Tirole, The RAND Journal of Economics **38**(1), 60 (2007), _eprint: https://onlinelibrary.wiley.com/doi/pdf/10.1111/j.1756-2171.2007.tb00044.x.
11. Geoffrey Haratyk, Energy Policy **110**, 150 (2017).
12. Abdalla Abou-Jaoude, Linyu Lin, Chandrakanth Bolisetti, Elizabeth Kirkpatrick Worsham, Levi Morin Larsen, Aaron S. Epiney, INL/RPT-23-72972-Rev000, Idaho National Laboratory (INL), Idaho Falls, ID (United States) (2023). https://www.osti.gov/biblio/1986466.
13. W. R. Stewart, K. Shirvan, Renewable and Sustainable Energy Reviews **155**, 111880 (2022).
14. Konor Frick, Daniel Wendt, Paul Talbot, Cristian Rabiti, Richard Boardman, Applied Energy **306**, 118044 (2022).
15. Manjur R Basnet, Jacob A Bryan, Seth J Dana, Aiden S Meek, Hailei Wang, Paul Talbot, Applied Energy **375**, 124105 (2024).
16. Daniel Hill, Adam Martin, Nathanael Martin-Nelson, Charles Granger, Matthew Memmott, Kody Powell, John Hedengren, International Journal of Thermofluids **16**, 100191 (2022).
17. Joshua W. Busby, Kyri Baker, Morgan D. Bazilian, Alex Q. Gilbert, Emily Grubert, Varun Rai, Joshua D. Rhodes, Sarang Shidore, Caitlin A. Smith, Michael E. Webber, Energy Research & Social Science **77**, 102106 (2021).
18. B. W. Dixon, F. Ganda, K. A. Williams, E. Hoffman, J. K. Hanson, INL/EXT-17-43826, Idaho National Lab. (INL), Idaho Falls, ID (United States) (2017). https://www.osti.gov/biblio/1423891.
19. U.S. Bureau of Labor Statistics, *Producer Price Index by Commodity: Construction (Partial): New Industrial Building Construction* (2007), Publisher: FRED, Federal Reserve Bank of St. Louis. https://fred.stlouisfed.org/series/WPU801104.
20. Jacopo Buongiorno, John Parsons, Michael Corradini, David Petti, , Massachusetts Institute of Technology (2018). https://energy.mit.edu/research/future-nuclear-energy-carbon-constrained-world/.
21. David Schlissel, *Eye-popping new cost estimates released for NuScale small modular reactor* (2023). https://ieefa.org/resources/eye-popping-new-cost-estimates-released-nuscale-small-modular-reactor.
22. SMR Start, *The Economics of Small Reactors* (2021). http://smrstart.org/wp-content/uploads/2021/03/SMR-Start-Economic-Analysis-2021-APPROVED-2021-03-22.pdf.
23. David Eugene Holcomb, Fred J. Peretz, A. L. Qualls, ORNL/TM-2011/364, Oak Ridge National Lab. (ORNL), Oak Ridge, TN (United States) (2011). https://www.osti.gov/biblio/1025856.
24. Anastasia Gandrik, Bruce Wallace, Michael Patterson, Phillip Mills, Technical TEV-1196, Idaho National Laboratory, Idaho Falls, ID (2012). https://art.inl.gov/NGNP/INL%20Documents/Year%202012/Assessment%20of%20High%20Temperature%20Gas-Cooled%20Reactor%20-%20HTGR%20-%20Capital%20and%20Operating%20Costs.pdf.
25. W. R. Stewart, E. Velez-Lopez, R. Wiser, K. Shirvan, Applied Energy **304**, 117650 (2021).
26. Gas-Cooled Reactor Associates, DOE-HTGR-90365 (1993). https://www.osti.gov/servlets/purl/10198837.
27. Eric Ingersoll, Kirsty Gogan, John Herter, Andrew Foss, , LucidCatalyst LLC, Cambridge, MA (United States) (2020). https://www.lucidcatalyst.com/the-eti-nuclear-cost-drivers.
28. Lazard, , Lazard (2023). https://www.lazard.com/research-insights/2023-levelized-cost-of-energyplus/.
29. J. R. Engel, H. F. Bauman, J. F. Dearing, W. R. Grimes, H. E. McCoy, W. A. Rhoades, ORNL/TM-7207, Oak Ridge National Lab. (ORNL), Oak Ridge, TN (United States) (1980). https://www.osti.gov/biblio/5352526.
30. X Energy Reactor Company, LLC, *X-energy Investor Presentation* (2023). https://x-energy.com/investors.

31. SM Short, BE Schmitt, , Pacific Northwest National Laboratory, Richland, WA (2018). https://albertainnovates.ca/wp-content/uploads/2020/07/Pacific-Northwest-National-Laboratory-Deployability-of-Small-Modular-Nuclear-Reactors-for-Alberta-Applications-Phase pdf.
32. Andrew Foss, Haydn C. Bryan, Jeremiah Pisarra, INL/LTD-21-01565, Idaho National Laboratory, Idaho Falls, ID (2021).
33. Seth Kirshenberg, Hilary Jackler, Jane Eun, Brian Oakley, Wil Goldenberg, , Allegheny Science & Technology Corporation (2017). https://www.energy.gov/ne/articles/small-modular-reactors-adding-resilience-federal-facilities.
34. U.S. Energy Information Administration, , U.S. Energy Information Administration (2020). https://www.eia.gov/analysis/studies/powerplants/capitalcost/.
35. W. Robb Stewart, Enrique Velez, Ralph Wiser, Koroush Shirvan, in *Energy Proceedings*, p. 6. https://www.energy-proceedings.org/?p=6880.
36. F. Ganda, FCRD-FCO-2015-000013, Argonne National Laboratory, Argonne, IL (United States) (2015). https://www.osti.gov/biblio/1555293.
37. F. Ganda, T. A. Taiwo, T. K. Kim, NTRD-FCO-2018-000439, Argonne National Lab. (ANL), Argonne, IL (United States) (2018). https://www.osti.gov/biblio/1464633.
38. David E. Shropshire, INL/EXT-09-15483, Idaho National Lab. (INL), Idaho Falls, ID (United States) (2009). https://www.osti.gov/biblio/957561.
39. Ch E. Boardman, p. 15. https://www.osti.gov/etdeweb/biblio/20248984.
40. EA Hoffman, RN Hill, TA Taiwo, in *Transactions of the American Nuclear Society*, (American Nuclear Society2004), pp. 768–769. https://www.ans.org/pubs/transactions/article-4728/.
41. National Renewable Energy Laboratory, *Electricity Annual Technology Baseline (ATB) Data Download* (2023). https://atb.nrel.gov/electricity/2022/data.
42. Daniel Mikkelson, Konor Frick, Shannon Bragg-Sitton, J. Michael Doster, Nuclear Technology **208**(3), 437 (2022), Publisher: Taylor & Francis _eprint: https://doi.org/10.1080/00295450.2021.1906473.
43. Lane T. Knighton, Amey Shigrekar, Daniel S. Wendt, Konor L. Frick, Richard D. Boardman, Amgad A. Elgowainy, Adarsh Bafana, Hla Tun, Krishna R. Reddi, INL/EXT-21-62939-Rev000, Idaho National Lab. (INL), Idaho Falls, ID (United States) (2021). https://www.osti.gov/biblio/1834404.
44. Paul W. Talbot, Abhinav Gairola, Prerna Prateek, Andrea Alfonsi, Cristian Rabiti, Richard D. Boardman, INL/EXT-19-56933-Rev000, Idaho National Lab. (INL), Idaho Falls, ID (United States) (2019). https://www.osti.gov/biblio/1581179.
45. Cristian Rabiti, Andrea Alfonsi, Diego Mandelli, Joshua J. Cogliati, Congjian Wang, Paul W. Talbot, Daniel P. Malijovec, Robert A. Kinoshita, Mohammad Gamal Abdo, Sonat Sen, Jun Chen, INL/EXT-15-34123-Rev.07, Idaho National Lab. (INL), Idaho Falls, ID (United States) (2021). https://www.osti.gov/biblio/1784874.
46. Georgios Mavromatidis, Kristina Orehounig, Jan Carmeliet, Applied Energy **214**, 219 (2018).
47. Seth J Dana, Aiden S Meek, Jacob A Bryan, Manjur R Basnet, Hailei Wang, Energy Storage **6**(4), e672 (2024).
48. I. M Sobol, Mathematics and Computers in Simulation **55**(1), 271 (2001).
49. A. Zakaria, Firas B. Ismail, M. S. Hossain Lipu, M. A. Hannan, Renewable Energy **145**, 1543 (2020).
50. Dylan James McDowell, Paul W. Talbot, Anna Marie Wrobel, Konor L. Frick, Haydn C. Bryan, Chad Boyer, Richard D. Boardman, John Taber, Jason K. Hansen, , Idaho National Lab.(INL), Idaho Falls, ID (United States) (2021). https://www.osti.gov/biblio/1844211.
51. Paul W. Talbot, Cristian Rabiti, Andrea Alfonsi, Cameron Krome, M. Ross Kunz, Aaron Epiney, Congjian Wang, Diego Mandelli, International Journal of Energy Research **44**(10), 8144 (2020), _eprint: https://onlinelibrary.wiley.com/doi/pdf/10.1002/er.5115.
52. Jun Chen, Cristian Rabiti, Energy **120**, 507 (2017).
53. Pierre Ailliot, Valérie Monbet, Environmental Modelling and Software **30**, 92 (2012), Publisher: Elsevier.
54. Dogan Keles, Massimo Genoese, Dominik Möst, Wolf Fichtner, Energy Economics **34**(4), 1012 (2012).
55. Bartosz Uniejewski, Rafal Weron, Florian Ziel, IEEE Transactions on Power Systems **33**(2), 2219 (2018).
56. Robert B Cleveland, William S Cleveland, Jean E McRae, Irma Terpenning, J. Off. Stat **6**(1), 3 (1990).
57. John E. Angus, SIAM Review **36**(4), 652 (1994), Publisher: Society for Industrial and Applied Mathematics.
58. B. Efron, R. Tibshirani, Statistical Science **1**(1), 54 (1986), Publisher: Institute of Mathematical Statistics.
59. Hans R. Kunsch, The Annals of Statistics **17**(3), 1217 (1989), Publisher: Institute of Mathematical Statistics.
60. Dimitris N. Politis, Joseph P. Romano, Journal of the American Statistical Association **89**(428), 1303 (1994), Publisher: Taylor & Francis _eprint: https://doi.org/10.1080/01621459.1994.10476870.
61. Dimitris N. Politis, Tucker S. McElroy, *Time Series: A First Course with Bootstrap Starter*, (CRC Press2019), Google-Books-ID: VorCDwAAQBAJ.
62. Dimitris N. Politis, Halbert White, Econometric Reviews **23**(1), 53 (2004), Publisher: Taylor & Francis _eprint: https://doi.org/10.1081/ETC-120028836.